ROYAL SOCIETY OF CHEMISTRY

Journal Name

COMMUNICATION

M³⁺O(-Mn⁴⁺)₂ Clusters in Doped MnOₓ Catalysts as Promoted Active Sites for Aerobic Oxidation of 5-Hydroxymethylfurfural

Kai Yu,*[ab‡] Yaqi Liu,[a‡] Da Lei,[ac] Yuanzhi Jiang,[c] Yanbing Wang,[c] Yajun Feng,[a] Lan-Lan Lou,[bc] Shuangxi Liu,*[cd] and Wuzong Zhou*[b]

Based on variuous experimental results, M³⁺O(-Mn⁴⁺)₂ clusters in (Fe, Co, Ni)-doped MnOₓ catalysts were identified as principal active sites for aerobic oxidation of 5-hydroxymethylfurfural due to their special property that makes oxygen to be easy come, easy go.

Noble-metal-free binary and ternary metal oxide catalysts are widely investigated and used in the aerobic oxidation of various substrates. However, to identify catalytically active sites in these oxides and electron transfer processes inside the active sites, and between catalyst and reactant in many catalytic systems are still challenging targets. Herein, we try to reveal active sites in doped MnOₓ for aerobic oxidation of 5-hydroxymethylfurfural (HMF) to 2,5-furandicarboxylic acid (FDCA).

This reaction, as a key reaction from biomass platform molecules to high value-added chemicals, has received much attention in the last decade.[1] Compared with the commonly used noble metal catalysts,[2] the noble-metal-free heterogeneous catalysts exhibit promising potential in industrial application due to their low costs. Compared with those reported noble-metal-free catalysts, such as Cu-MOR supported vanadium oxide[3] and nano-Fe₃O₄-CoOₓ,[4] MnO₂ was found to be catalytically active in the aerobic oxidation of HMF towards FDCA using O₂ as the oxidant in aqueous medium,[5] which is more attractive when the environmental benefit is considered. However, the properties of the catalysts vary in a wide range and our knowledge of the relevant catalytic mechanisms is still limited.

In the present work, MnOₓ nanowires with transition metal (M = Fe, Co, Ni) doping were prepared and served as efficient catalysts for the aerobic oxidation of HMF to FDCA. Based on the observed influence of the doping on the catalytic performance of MnOₓ, and the corresponding ratios of M^{3+}/M^{2+} and Mn^{4+}/Mn^{3+}, we propose that the promoted performance is associated with formation of catalytically active clusters, M³⁺O(-Mn⁴⁺)₂. The mechanism of the catalytic aerobic oxidation of HMF is therefore better understood.

Fe-, Co-, and Ni-doped MnOₓ nanowires were prepared, according to a previous report,[6] in a hydrothermal treatment of a solution of $MnSO_4$, $(NH_4)_2S_2O_8$, $(NH_4)_2SO_4$ and MSO_4 (M = Fe, Co or Ni) at 140 °C for 12 h, followed by calcination of the pre-dried specimens at 200 °C in air for 3 h. The samples are designated as M-MnOₓ. Undoped MnOₓ nanowires were also synthesised under the same conditions without adding the guest cations. The details of the synthesis conditions together with the characterization methods are given in ESI†. The actual doping levels of ~5% were detected by inductively coupled plasma-atomic emission spectrometry (ICP-AES), as listed in Table S1, ESI†.

Initial characterization of the samples was by powder X-ray diffractometry (XRD). All the diffraction peaks of the synthesised samples can be indexed onto the body centred tetragonal phase of α-MnO₂ with $a = 0.9784$ and $c = 0.2863$ nm, space group I4/m (JCPDS 44-0141) (Fig. S1a, ESI†). No crystalline impurities nor superstructures were detected. Due to larger cation radii of Fe^{2+}(0.92 Å), Co^{2+}(0.89 Å) and Ni^{2+}(0.83 Å) than Mn^{4+}(0.67 Å) or Mn^{3+}(0.79 Å), the XRD peaks of the doped oxides slightly shift to lower 2θ (Fig. S1b, ESI†), confirming a solid solution state.

All the particles appear as nanowires with an average width of ~20 nm and a length over 600 nm, as detected using scanning electron microscopy (SEM) and transmission electron microscopy (TEM). High resolution TEM (HRTEM) images confirm the MnO₂-type structure. The formation mechanism of the nanowire morphology can be understood by realising a fast growth rate along the c axis with a very small d-spacing of

a. MOE Key Laboratory of Pollution Processes and Environmental Criteria, College of Environmental Science and Engineering, Nankai University, Tianjin 300350, China. E-mail: kaiyu@nankai.edu.cn.
b. School of Chemistry, University of St Andrews, St Andrews, Fife KY16 9ST, UK. E-mail: wzhou@st-andrews.ac.uk.
c. Institute of New Catalytic Materials Science and MOE Key Laboratory of Advanced Energy Materials Chemistry, School of Materials Science and Engineering, National Institute of Advanced Materials, Nankai University, Tianjin 300350, China. E-mail: sxliu@nankai.edu.cn.
d. Collaborative Innovation Center of Chemical Science and Engineering (Tianjin), Tianjin 300072, China.
† Electronic Supplementary Information (ESI) available: Experimental section, characterisation results and catalytic properties. See DOI: 10.1039/x0xx00000x
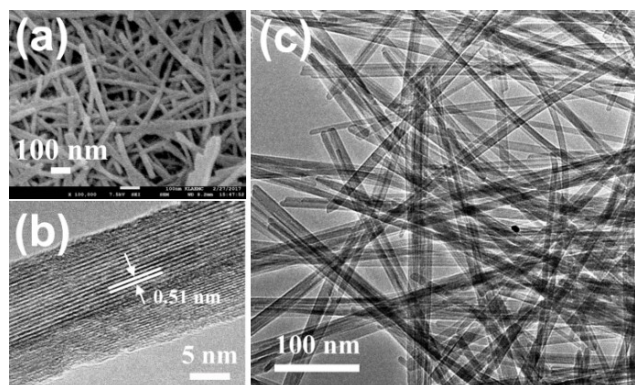‡ These authors contributed equally to this work.

Fig. 1. (a) SEM, (b) HRTEM, and (c) TEM images of Ni-MnOx nanowires. The measured d-spacing of 0.51 nm corresponds to the (200) planes in the MnO_2-type unit cell.

Fig. 2. (a) Mn 2p and (b) O 1s XPS spectra of M-MnOx and MnOx nanowires. The ratio of Mn^{4+}/Mn^{3+} and proportion of surface chemisorbed oxygen $O_\alpha/(O_\alpha+O_\beta)$ are given in (a) and (b), respectively. (c) Ni 2p XPS spectrum of Ni-MnOx nanowires.

(002).[7] The images from samples with different compositions are very similar (Fig. 1 and Fig. S2, ESI†). Energy dispersive X-ray (EDX) elemental mapping indicates that all the guest cations are evenly distributed in the nanowires (Fig. S3, ESI†).

In order to investigate the valence states of Mn and O ions in the near surface areas, X-ray photoelectron spectroscopy (XPS) of the nanowires was performed. In the Mn 2p XPS spectra of these samples (Fig. 2a), two peaks located at *ca.* 641.9 and 653.5 eV can be attributed to the spin orbit doublet of Mn $2p_{3/2}$ and Mn $2p_{1/2}$. The overlapped Mn 2p peaks can be deconvoluted into several sub-bands using CasaXPS processing software. The major components at 642.1 and 653.8 eV can be attributed to Mn^{4+}, while the minor components at 641.3 and 653.0 eV indicate the existence of Mn^{3+} in manganese oxide.[7] The ratio of Mn^{4+}/Mn^{3+} (Fig. 2a) is 2.53 in MnOx indicating a high concentration of Mn^{3+}. As shown in Fig. 2a, the doped MnOx have higher ratios of Mn^{4+}/Mn^{3+} with the highest (5.11) in Ni-MnOx.

O 1s XPS was employed to investigate the surface oxygen species of the specimens. The spectra can be deconvoluted to three peaks (Fig. 2b). The weak peak at the highest binding energy of 532-533 eV can be attributed to the absorbed water on the surface. The peak at relatively lower binding energy of 529-530 eV corresponds to the lattice O^{2-} (denoted as O_β), and the peak at 531-532 eV is assigned to the reactive oxygen species, such as O_2^-, O_2^{2-}, and O^- (denoted as O_α).[8] The ratio of $O_\alpha/(O_\alpha+O_\beta)$ is calculated from the areas of the two peaks. M-MnOx, with higher values of $O_\alpha/(O_\alpha+O_\beta)$, exhibit notably improved oxygen activation capacity than MnOx. Among them, Ni-MnOx exhibits the highest capacity (Fig. 2b).

It is commonly accepted that the oxygen activation capacity of metal oxide is closely related to the oxygen vacancies in the crystals. In the present work, however, it is interesting to see that Ni-MnOx with the lowest amount of Mn^{3+}, and therefore the lowest amount of oxygen vacancies, exhibits the highest amount of reactive oxygen species. The effect of doping and the role of the guest cations in catalysis must be re-investigated.

There are a large amount of Mn^{3+}, associated with oxygen vacancies in the parent MnOx, as indicated by the low ratio (2.53)
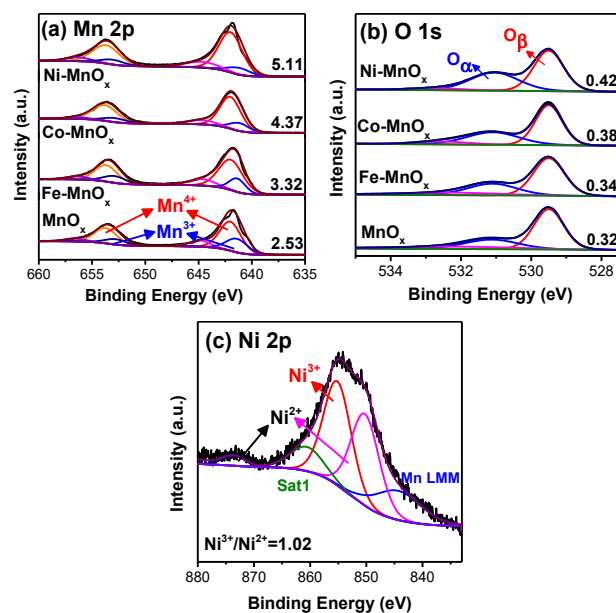
of Mn^{4+}/Mn^{3+} (Fig. 2a). Taking Ni-MnOx as example, Ni^{2+} would preferentially substitute Mn^{3+} rather than Mn^{4+} due to their close radii and charge states, forming a cluster with an oxygen vacancy, $Ni^{2+}\square(-Mn^{3+})_2$. On the other hand, the oxygen vacancies associated with these sites might be filled to form stable NiO_6 octahedra,[9] which partially share edges in the MnO_2 matrix, giving a suitable environment for Ni^{3+} cations. Consequently, the cations at these sites would be oxidised, forming $Ni^{3+}O(-Mn^{4+})_2$ clusters. As a result, the guest cations exist as 2+ and 3+ cations in these M-MnOx nanowires, as shown in the M 2p XPS spectra (Fig. 2c and Fig. S4, ESI†). Indeed, the doping increases the ratio of Mn^{4+}/Mn^{3+} and reduces the number of oxygen vacancies, both being related to the formation of the $Ni^{3+}O(-Mn^{4+})_2$ clusters.

O_2 temperature-programmed desorption (O_2-TPD) was also carried out. Two desorption peaks of O_2 are recognized (Fig. 3a). The low-temperature peak (300-450 °C) can be attributed to the surface reactive oxygen species,[8] and the wide high-temperature peak (450-600 °C) corresponds to the release of the surface lattice oxygen.[10] All the doped specimens exhibit increased peak intensity in the low-temperature region, indicating a notably enhanced oxygen activation capacity with the doping. The results are consistent with the O 1s XPS results. In addition, the oxygen desorption peak in the high-temperature region shifts from 562 °C (MnOx) to 523 °C (Ni-MnOx), implying that the doping enhances desorption of surface lattice oxygen as well. One reason for this phenomenon is that the oxygen in the $Ni^{3+}O(-Mn^{4+})_2$ clusters are quite different from the lattice oxygen in MnOx, but are mobile active lattice oxygen. In other words, oxygen anions in these clusters intend to leave in order to keep the charge balance with Ni^{3+}.
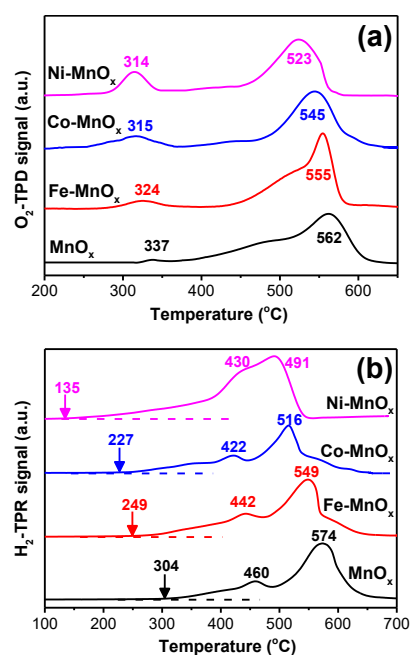
Fig. 3. (a) The O_2-TPD and (b) H_2-TPR profiles of the M-MnO_x and MnO_x nanowires.

In order to evaluate the redox property of the samples, H_2 temperature-programmed reduction (H_2-TPR) has been also performed (Fig. 3b). Three reduction peaks can be observed from MnO_x in the temperature region from 300 °C to 650 °C, corresponding to three sequential reduction processes, MnO_2 to Mn_2O_3, Mn_2O_3 to Mn_3O_4, and Mn_3O_4 to MnO, respectively.[11] With the doping, the reduction peaks shift to lower temperatures, suggesting that the incorporation of the guest cations effectively promotes the reduction of MnO_x. Especially, Ni-MnO_x shows the lowest initial reduction temperature at 135 °C. The notably decreased reduction temperature was previously believed to be mainly attributed to the easier reduction of uniformly dispersed guest cations and associated with distortion of the MnO_2 structure.[12] In the newly established model, as discussed below in detail, easy removal of the oxygen coordinating the guest cations is probably the more direct reason.

The nanowires were evaluated in the aerobic oxidation of HMF (Table 1). A typical reaction profile over Ni-MnO_x is given in Fig. S5 (ESI†). It can be seen that all the samples are active under this reaction condition. The main products are FFCA and FDCA without detectable DFF and HMFCA. The highest yield of FDCA (93.8%) was achieved by using Ni-MnO_x. The order of catalytic activity of these nanowires is Ni-MnO_x > Co-MnO_x > Fe-MnO_x > MnO_x, which is consistent with the order of their oxygen activation capacity and redox property. MnO_x shows notably lower catalytic activity in comparison with M-MnO_x, but it is still higher than the commercial MnO_2 material, suggesting the amount of high valence state of Mn ions is not the key factor for the promotion of catalytic performance. It is noticed that ~7% HMF was converted to by-products over all the samples, which can be mainly attributed to the ketonization and condensation reaction of products.[13]

Table 1. The catalytic performance of MnO_x and M-MnO_x nanowires in aerobic oxidation of HMF.[a]

Catalyst	Conv. of HMF (%)	Yield (%)				
		DFF	HMFCA	FFCA	FDCA	Others
Ni-MnO_x	100	0	0	0	93.8	6.2
Co-MnO_x	100	0	0	8.3	84.5	7.2
Fe-MnO_x	100	0	0	14.1	78.6	7.3
MnO_x	100	0	0	20.0	72.8	7.2
MnO_2 [b]	100	0	0	35.9	56.7	7.4

[a] Reaction conditions: HMF (0.126 g), $NaHCO_3$ (0.336 g), catalyst (0.1 g), H_2O (10.0 mL), 100 °C, O_2 (0.8 MPa), 28 h. [b] Commercial MnO_2.

If the guest cations are involved in the active sites for the promotion of the catalytic performance, the influence of their concentrations must be interesting. Ni-MnO_x nanowires with different doping were prepared with the molar ratio, Mn/Ni, of R, (R = 5, 10, and 15), designated as Ni-MnO_x(R). The actual Ni contents determined by ICP-AES were 11.45, 4.95, and 2.24% as listed in Table S2, ESI†. It can be seen from Table S3 in ESI† that Ni-MnO_x(10) exhibits the highest catalytic performance. The yield of FDCA increases from 87.7% of Ni-MnO_x(15) to 93.8% of Ni-MnO_x(10), but reduces with further doping to 80.8% of Ni-MnO_x(5).

High resolution XPS in the core level regions of Mn 2p and O 1s (Fig. S6, ESI†) show that both the values of Mn^{4+}/Mn^{3+} and $O_\alpha/(O_\alpha+O_\beta)$ in these specimens do not increase monotonically with the increase of the Ni doping. Ni-MnO_x(10) exhibits the highest value of $O_\alpha/(O_\alpha+O_\beta)$, 0.42 against 0.37 of Ni-MnO_x(15) and 0.35 of Ni-MnO_x(5), and the highest Mn^{4+}/Mn^{3+}, 5.10 against 4.63 of Ni-MnO_x(15) and 4.11 of Ni-MnO_x(5) (Table S2, ESI†). These results support the model of the proposed active sites of $Ni^{3+}O(-Mn^{4+})_2$, since when the doping level of Ni is too high, some larger clusters containing Ni-O-Ni would form, leading to a reduction of Mn^{4+} and stabilization of the oxygen anions bonding to 2 or 3 Ni. Furthermore, the extremely lower catalytic activity of NiO or Ni_2O_3 in aerobic oxidation of HMF compared with Ni-MnO_x and MnO_x further indicated that the role of Ni cations in promoting of catalytic activity of Ni-MnO_x is the formation of $Ni^{3+}O(-Mn^{4+})_2$ clusters.

Based on the above discussion, a new reaction mechanism of aerobic oxidation of HMF on M-MnO_x nanowires is proposed as shown in Fig. 4. Taking Ni-MnO_x as an example, each oxygen in the MnO_2–type structure is coordinated by three metal cations and therefore contributes 2/3– charge per chemical bond to the cations. Each Ni^{3+} gains 4– charge from 6 coordinated oxygen. The unbalanced charge at Ni^{3+} reduces the stability of the oxygen in a $Ni^{3+}O(-Mn^{4+})_2$ cluster, which has a potential to dissociate, generating a vacancy. This process becomes much easier when the cluster is located at the surface region of a crystal, e.g. offering the oxygen atom to HMF. At the same time, Mn^{4+} and Ni^{3+} in the cluster are reduced to Mn^{3+} and Ni^{2+} by receiving electrons from oxygen, forming a $Ni^{2+}\square(-Mn^{3+})_2$ cluster. On the other hand, the formation of the oxygen vacancy would inevitably cause lattice distortion and less favourable coordination for Ni. Consequently, the oxygen vacancy in

$Ni^{2+}\square(-Mn^{3+})_2$ has a potential to adsorb oxygen again, showing an excellent regenerative ability of active lattice oxygen. In other words, the $Ni^{2+}\square(-Mn^{3+})_2$ clusters offer active sites for oxygen to be easy come, easy go.
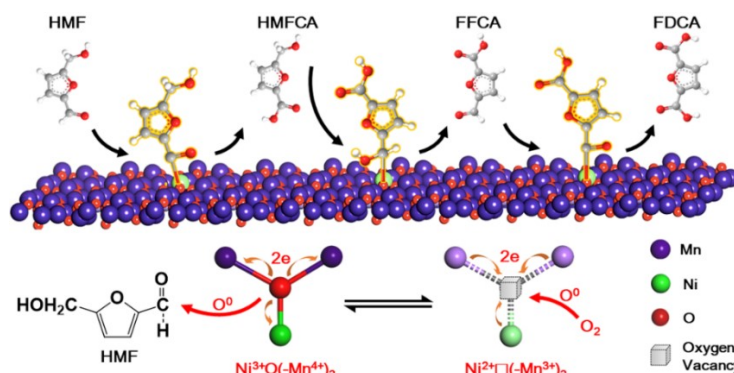

Fig. 4. Top: proposed reaction mechanism for aerobic oxidation of HMF to FDCA on $Ni^{3+}O(-Mn^{4+})_2$ clusters in Ni-MnO$_x$ nanowires. Bottom: Schematic drawing to show change from a $Ni^{3+}O(-Mn^{4+})_2$ cluster to a $Ni^{2+}\square(-Mn^{3+})_2$ cluster via losing the oxygen atom and electron transfer from oxygen to the cations, and restoring $Ni^{3+}O(-Mn^{4+})_2$ via receiving oxygen and electron transfer from the cations to oxygen.

It is very different with the viewpoint of reported works,[5] which believed that the surface Mn^{4+} ions or corresponded lattice oxygen acted as the active sites, or the synergetic cooperation of Mn^{3+} and Mn^{4+} coexists with a hematite phase in mixed Mn/Fe oxides played a key role in noble-metal-free aerobic oxidation of HMF. In the present work, we believe that the asymmetrical $M^{3+}O(-Mn^{4+})_2$ clusters act as the active sites, which can continuously provide active lattice oxygen species through the circle between $M^{3+}O(-Mn^{4+})_2$ and $M^{2+}\square(-Mn^{3+})_2$ because of the unbalanced charge or unfavourable coordination of two states of these clusters. On the surface area of catalysts, the oxygen in the active sites may reduce its coordination number from 3 to 2, leading to M^{3+}-O-Mn^{4+}. But the function should be the same.

In order to prove the superior oxidizability of $Ni^{3+}O(-Mn^{4+})_2$ clusters compared with symmetric $Mn^{4+}O(-Mn^{4+})_2$ clusters, a density functional theory (DFT) theoretically calculation on the energy of oxygen release from these clusters were performed and the results are shown in Fig. S7 of ESI†. It can be found that the oxygen atoms in asymmetric $Ni^{3+}O(-Mn^{4+})_2$ clusters exhibited notably lower energy of oxygen release compared with symmetric $Mn^{4+}O(-Mn^{4+})_2$ clusters, no matter what the coordination number of oxygen in these clusters is 2 or 3. It indicated the higher oxidizability of $Ni^{3+}O(-Mn^{4+})_2$ clusters in the oxidation reaction.

In the reaction process of aerobic oxidation of HMF, the active lattice oxygen in $Ni^{3+}O(-Mn^{4+})_2$ cluster attacks the aldehyde group of HMF, forming HMFCA with a carboxylic group, leaving a vacancy and reduced cations in a $Ni^{2+}\square(-Mn^{3+})_2$ cluster. This vacancy can be soon re-filled by an oxygen atom from O$_2$, taking back electrons from the cations. The $Ni^{3+}O(-Mn^{4+})_2$ cluster is therefore recovered (Fig. 4). Then, the hydroxymethyl group of HMFCA approaches to the active oxygen in a $Ni^{3+}O(-Mn^{4+})_2$ cluster, adopts the oxygen to form diol group and further produces the FFCA via dehydration. The third step is similar to step 1: the aldehyde group of FFCA is oxidized, leading to formation of FDCA.

During the circle of these two states (see bottom of Fig. 4), the basic structure is maintained. Consequently, a long life time of the catalysts can be expected. The reusability of Ni-MnO$_x$ has been tested via the cycling catalytic reactions for 28 h each run (Fig. S8, ESI†). After each cycling experiment, the catalyst was collected by centrifuge and washed with water, then dried for the next run. It can be found that the catalytic performance of Ni-MnO$_x$ exhibits a slightly decrease at the first three cycles, the yield of FDCA decrease from 93.8% to 87.3% for the 3rd run. The XRD pattern of the used catalyst (Fig. S9, ESI†) indicates that no serious destruction in the crystal structure took place. The Mn 2p and O 1s XPS spectra of the used catalyst after 3 cycles (Fig. S10, ESI†) show that the molar ratio of Mn^{4+}/Mn^{3+} and the content of surface chemisorbed oxygen species (O$_\alpha$) decrease obviously, suggesting part of $Ni^{3+}O(-Mn^{4+})_2$ clusters have been reduced to $Ni^{2+}\square(-Mn^{3+})_2$ after the oxidation reaction. The O$_2$-TPD characterization of used Ni-MnO$_x$ catalysts (Fig. S11, ESI†) exhibits the similar results. The intensity of O$_2$ desorption peak in the low-temperature region decreases obviously, suggesting a decrease of surface chemisorbed oxygen species on the surface of used Ni-MnO$_x$ catalyst, which is consistent with the results of O 1s XPS. The reason for the reduced redox property and recyclability is that the replenishment of active lattice oxygen species on these sites is slower than the consumption of them. On the other hand, when the catalyst was calcined at 200 ºC in air for 3 h after the 3rd run, the yield of FDCA was restored to 92.1% at the 4th run, suggesting the restore of $Ni^{3+}O(-Mn^{4+})_2$ clusters. A stable catalytic activity lasted at least 7 times through a facilitated calcination treatment every 3 cycles, demonstrating that the sample still has a high reusability.

In summary, in the investigation of catalytic activities of Ni, Co and Fe-doped MnO$_x$ nanowires in aerobic oxidation of HMF to FDCA, we identified active clusters $M^{3+}O(-Mn^{4+})_2$, in which active oxygen can be easy come, easy go at the metastable sites. All the experimentally observed phenomena can be explained using these active sites. This work may provide insights into the

mechanism on electron transfer inside the catalytically active sites in catalytic processes on many other binary and ternary metal oxide catalysts.

Notes and references

1   M. E. Zakrzewska, E. Bogel-Łukasik and R. Bogel-Łukasik, *Chem. Rev.,* 2011, **111**, 397–417; Z. Zhang and K. Deng, *ACS Catal.,* 2015, **5**, 6529–6544.

2   D. Lei, K. Yu, M.-R. Li, Y. Wang, Q. Wang, T. Liu, P. Liu, L.-L. Lou, G. Wang and S. Liu, *ACS Catal.*, 2017, **7**, 421–432.; Y. Wang, K. Yu, D. Lei, W. Si, Y. Feng, L.-L. Lou and S. Liu, *ACS Sustainable Chem. Eng.,* 2016, **4**, 4752–4761.

3   W. Zhang, J. Xie, W. Hou, Y. Liu, Y. Zhou and J. Wang, *ACS Appl. Mater. Inter.,* 2016, **8**, 23122–23132.

4   S. Wang, Z. Zhang and B. Liu, *ACS Sustain. Chem. Eng.,* 2015, **3**, 406–412.

5   F. Neaţu, R. S. Marin, M. Florea, N. Petrea, O. D. Pavel and V. I. Pârvulescu, *Appl. Catal. B: Environ.,* 2016, **180**, 751–757; E. Hayashi, T. Komanoya, K. Kamata and M. Hara, *ChemSusChem,* 2017, **10**, 654–658; X. Han, C. Li, X. Liu, Q. Xia and Y. Wang, *Green Chem.,* 2017, **19**, 996–1004.

6   X. Wang and Y. Li, *Chem. -Eur. J.,* 2003, **9**, 300–306; Z. Wang, F. Wang, Y. Li, J. Hu, Y. Lu and M. Xu, *Nanoscale,* 2016, **8**, 7309–7317.

7   N. Jabeen, Q. Xia, S. V. Savilov, S. M. Aldoshin, Y. Yu and H. Xia, *ACS Appl. Mater. Inter.,* 2016, **8**, 33732–33740.

8   Y. Chen, H. Zheng, Z. Guo, C. Zhou, C. Wang, A. Borgna and Y. Yang, *J. Catal.* 2011, **283**, 34–44; S. Zhan, H. Zhang, Y. Zhang, Q. Shi, Y. Li and X. Li, *Appl. Catal. B: Environ.,* 2017, **203**, 199–209.

9   S.-D. Ouyang, Y.-M. Quan, D.-Y. Liu and L.-J. Zou, *Chin. Phys. Lett.,* 2011, **28**, 067102.

10 B. Zhang, G. Cheng, B. Lan, X. Zheng, M. Sun, F. Ye, L. Yu and X. Cheng, *CrystEngComm*, 2016, **18**, 6895–6902.

11 B. Thirupathi and P. G. Smirniotis, *Appl. Catal. B: Environ.,* 2011, **110**, 195–206.

12 J. Gao, C. Jia, L. Zhang, H. Wang, Y. Yang, S.-F. Hung, Y.-Y. Hsu and B. Liu, *J. Catal.,* 2016, **341**, 82–90.

13 O. Casanova, S. Iborra and A. Corma, *ChemSusChem*, 2009, **2**, 1138–1144; S. E. Davis, L. R. Houk, E. C. Tamargo, A. K. Datye and R. J. Davis, *Catal. Today,* 2011, **160**, 55–60; Z. Du, J. Ma, F. Wang, J. Liu and J. Xu, *Green Chem.,* 2011, **13**, 554–557.

The Table of Contents (TOC)

$M^{3+}O(-Mn^{4+})_2$ Clusters in Doped MnO_x Catalysts as Promoted Active Sites for Aerobic Oxidation of 5-Hydroxymethylfurfural

Kai Yu, Yaqi Liu, Da Lei, Yuanzhi Jiang, Yanbing Wang, Yajun Feng, Lan-Lan Lou, Shuangxi Liu and Wuzong Zhou

$M^{3+}O(-Mn^{4+})_2$ clusters in (Fe, Co, Ni)-doped MnO_x catalysts were identified as principal active sites for aerobic oxidation of 5-hydroxymethylfurfural due to their special property that makes oxygen to be easy come, easy go.